Rapid Communications

Role of flexural stiffness of leukocyte microvilli in adhesion dynamics

Tai-Hsien Wu* and Dewei Qi†
Department of Chemical and Paper Engineering, Western Michigan University, Kalamazoo, Michigan 49008, USA

(Received 15 November 2017; published 1 March 2018)

Previous work reported that microvillus deformation has an important influence on dynamics of cell adhesion. However, the existing studies were limited to the extensional deformation of microvilli and did not consider the effects of their bending deformation on cell adhesion. This Rapid Communication investigates the effects of flexural stiffness of microvilli on the rolling process related to adhesion of leukocytes by using a lattice-Boltzmann lattice-spring method (LLM) combined with adhesive dynamics (AD) simulations. The simulation results reveal that the flexural stiffness of microvilli and their bending deformation have a profound effect on rolling velocity and adhesive forces. As the flexural stiffness of the microvilli decreases, their bending angles increase, resulting in an increase in the number of receptor-ligand bonds and adhesive bonding force and a decrease in the rolling velocity of leukocytes. The effects of flexural stiffness on deformation and adhesion represent crucial factors involved in cell adhesion.

DOI: 10.1103/PhysRevFluids.3.031101

I. INTRODUCTION

Several direct simulation studies were performed to examine the influence of microvillus deformation on cell adhesion. Caputo and Hammer [1] improved Hammer and Apte's pioneering adhesive dynamics model [2] by using a spring to approximate the elastic extensional response to a small force of microvillus, as well as its plastic tethering response to a large force. Although Pawar *et al.* [3] further improved the model by replacing the hard spherical cell with a deformable neo-Hookean membrane, they kept the same extensional deformation of microvilli as that of Caputo and Hammer. Alternately, Khismatullin and Truskey [4] combined the microvillus spring with the receptor-ligand spring to express extensional deformation of microvilli and adhesive bonds. Later, Pospieszalska *et al.* [5] allowed the microvillus to pivot around its base but remain stretched, without considering bending stiffness and corresponding tangential elastic force. To the best of our knowledge, all the existing simulation work was limited to extensional deformation and force on the microvillus. These studies did not incorporate its bending stiffness and associated bending forces, as this study does.

In fact, when a force tangential to the cell surface is exerted on a leukocyte microvillus, the microvillus will be bent [6]. The bending of microvilli could potentially influence the binding between receptors and ligands. In particular, when microvilli are flattened with the cell surface, the receptors in the microvilli bases (instead of on the microvilli tips) may obtain additional adhesion with ligands on the endothelial cells (ECs) or on the ligand-coated substrate [7]. The flexibility increases as the flexural stiffness decreases. The flexibility of a microvillus may allow it to be more easily bent

*tai-hsien.wu@wmich.edu
†Corresponding author: dewei.qi@wmich.edu

and may facilitate the contacts between the receptors on the microvillus tip and the ligands on the endothelium, resulting in an increase in adhesion.

Due to the importance of flexibility in microvilli, Yao and Shao [8,9] measured experimentally the flexural stiffness of the microvilli on lymphocytes and neutrophils under small deformation of the microvilli. They reported that the values of the flexural stiffness of lymphocyte and neutrophil microvilli are 4 and 7 pN/μm, respectively [8,9]. Simon *et al.* [10] conducted another experiment to measure the flexural stiffness of a neutrophil microvillus under a large deformation (0.5–1 μm) and found that the flexural stiffness is 5 pN/μm.

To take account of the bending effects of microvilli, we employ the measured data of flexural stiffness to study the roles of flexural stiffness on cell rolling and adhesion by using a lattice-Boltzmann lattice-spring method (LLM) combined with adhesive dynamics (AD) simulations. This method treats not only extensional but also bending deformation of the microvilli. The method is comprised of five numerical models: (1) lattice-Boltzmann method (LBM) for the Navier-Stokes flow [11–24]; (2) coarse-grained cell model (CGCM) for the viscoelastic leukocyte membrane [25]; (3) lattice-spring model (LSM) for the flexible microvilli [26]; (4) immersed boundary method (IBM) for the fluid-cell interactions [27]; (5) adhesive dynamics (AD) for stochastic binding between P-selectin and P-selectin-glycoprotein-ligand-1 (PSGL-1) [2].

In the present work we use an elastic angular spring possessing a three-body force to approximate the bending deformation of microvilli. In addition, we use an elastic bonding spring which has a center-to-center two-body force responsible for extensional deformation. In order to focus attention on the bending effect only, the flexural stiffness of the angular spring varies at different levels, while the spring extensional stiffness is kept at a constant. The various physical quantities were calculated and used to characterize cell adhesion. This work will fill a gap in the area of adhesive dynamics simulations since there are no known reports on the effects of flexural stiffness of microvilli.

II. METHODS

A. Lattice Boltzmann method

The motion of Newtonian fluid is governed by the incompressible Navier-Stokes equations, and the LBM has been proven to satisfy the incompressible Navier-Stokes equations by solving the Boltzmann kinetic equation for Mach numbers below 0.3 [12–19]. The kinetic nature of the LBM makes it more suitable for simulating multicomponent flows such as blood [20–24]. We implement and use a parallel CUDA code [28] of the multi-relaxation-time LBM [11,29,30] and the associated the LLM in this work [31]. More details of the LBM can be found in the Supplemental Material, part A [32], and Refs. [12,13,33,34].

B. Coarse-grained cell model

The CGCM was presented by Fedosov *et al.* [25,35,36], in which a blood cell can be represented by a membrane. The membrane is discretized as individual solid particles, each with a mass M, and connected by a two-dimensional triangulated network. The total potential energy of the membrane has four terms and is written as

$$U^{\text{total}} = U^{\text{in-plane}} + U^{\text{area}} + U^{\text{volume}} + U^{\text{bending}}, \tag{1}$$

where the in-plane potential energy term $U^{\text{in-plane}}$ is described by a combination of the finitely extensible nonlinear elastic (FENE) and power law (POW) potential energies [37]; the energies U^{area} and U^{volume} are used to consider the conservation of cell surface area and volume; and the bending energy U^{bending} exists between two adjacent elements (four adjacent solid particles). Thus, the total elastic force on each particle can be computed. Further, the CGCM [25,36,37] also addresses the membrane's viscous property by adding a dissipative term to each spring. Finally, the leap-frog algorithm is used to update the positions and velocities of every solid particle at each time step.

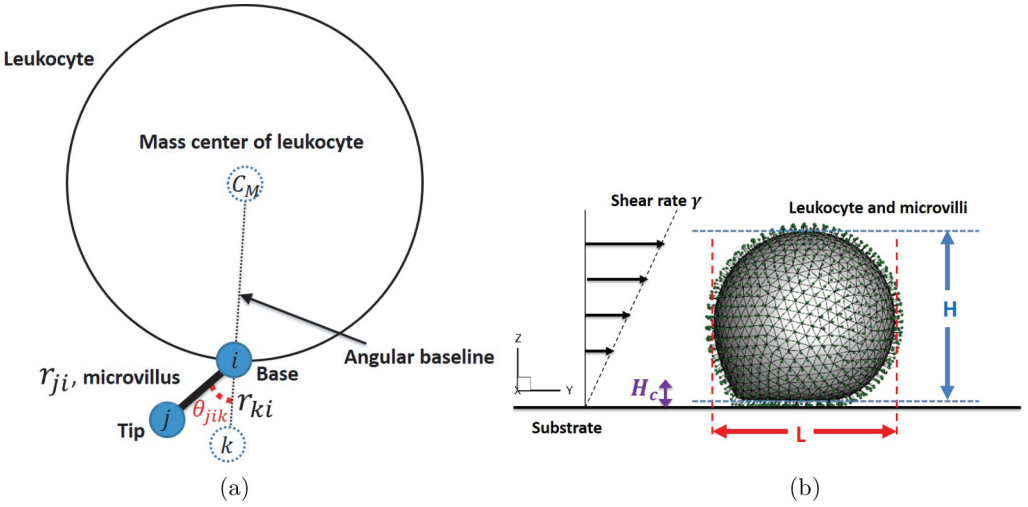

FIG. 1. (a) Schematic of the LSM for the microvilli. (b) Schematic of the simulation configuration.

C. Lattice-spring model

Wu *et al.* [26] reported a generalized LSM in which an extensional spring and an angular spring are used to account for extensional and bending deformation, respectively. We apply the LSM to mimic the deformation of the leukocyte microvilli. As shown in Fig. 1(a), a microvillus is modeled by a spring (vector $\mathbf{r}_{ji}$) with one end fixed at the base particle i (microvillus base) on the cell surface and with the other end j as the microvillus tip. Two types of deformation are illustrated. First, the tip particle j of the spring can be extended or compressed with respect to the base particle i. The potential energy responsible for the spring extension or compression U^s is given by

$$U^s = \tfrac{1}{2}k_s^{mv}(r_{ji} - r_{0ji})^2, \tag{2}$$

where r_{ji} and r_{0ji} are the instantaneous and initial microvillus lengths, respectively, and k_s^{mv} is the extensional spring constant. Second, vector $\mathbf{r}_{ji}$ can be bent with respect to vector $\mathbf{r}_{ki}$ to have a bending angle θ_{kij}, where k is always located on the extension portion of the line connecting the mass center C_M to the base particle i. The line is called the angular baseline [the dashed line in Fig. 1(a)] and is used for the measurement of the bending angle only. In fact, $\mathbf{r}_{ki}$ is a virtual bond, and particle k does not participate in simulation. The energy due to the bending bond U^a is written as

$$U^a = \tfrac{1}{2}k_a^{mv}(\theta_{kij} - \theta_{0kij})^2, \tag{3}$$

where k_a^{mv} is the angular spring constant and θ_{0kij} represents the equilibrium angle. The elastic force is calculated from the gradient of the sum of U^a and U^s with respect to solid particles i and j.

According to Refs. [8–10,38], the extensional stiffness and flexural stiffness of the microvilli are 152–1340 and 4–7 pN/μm, respectively. The flexural stiffness K is defined by a ratio of the force on the microvillus to the corresponding deflection, and it is related to the angular spring constant by $K = k_a^{mv}/L_{mv}^2$. The derivation of the relationship between flexural stiffness and angular spring constant is given in Supplemental Material, part B [32]. In this study, we first set k_s^{mv} as 1340 pN/μm and K as 7 pN/μm for validation, and then vary the flexural stiffness K to investigate the role of flexural stiffness in leukocyte adhesion.

D. Immersed boundary method

To ensure that the solid particle velocity is equal to the fluid particle velocity at the solid boundary, an interaction force on the fluid can be calculated from the momentum difference between the

boundary solid particle and unforced fluid velocities. The unforced fluid velocity is calculated from the surrounding fluid particles by using a discrete Dirac delta function [27]. Similarly, the interaction force is distributed into fluid by using the same function. More details can be found in the literature [26,27,31,34,39].

E. Adhesive dynamics

The AD was presented first by Hammer and Apte for simulation of leukocyte adhesion to endothelial cells (ECs) [2]. This method uses the stochastic Monte Carlo method and Dembo kinetics model to simulate the formation and rupture of the receptor-ligand bond.

In the Dembo model [40], the forward and reverse rates for the receptor-ligand bond under external force are written as follows:

$$k_f = k_f^0 \exp\left[-\frac{\sigma_{ts}(l-l_0)^2}{2K_BT}\right] \quad \text{and} \quad k_r = k_r^0 \exp\left[\frac{(\sigma_b-\sigma_{ts})(l-l_0)^2}{2K_BT}\right], \tag{4}$$

where k_f^0 and k_r^0 are the unstressed forward and reverse reaction rates, respectively; l and l_0 are the stretched and unstressed equilibrium bond lengths, respectively; σ_b and σ_{ts} are the spring constants in the bound and transition states, respectively; K_B is the Boltzmann constant; and T is the absolute temperature. The force F_b, acting on the receptor-ligand bond, is assumed to follow the Hookean spring model, which can be written as

$$F_b = \sigma_b(l-l_0). \tag{5}$$

The probabilities of formation of a new bond P_f and of rupture of an existing bond P_r in a time interval Δt are given by

$$P_f = 1-\exp(-k_{\text{on}}\Delta t) \quad \text{and} \quad P_r = 1-\exp(-k_r\Delta t), \tag{6}$$

where $k_{\text{on}} = k_f A_L(n_L - n_b)$; A_L is the local surface area on the ligand-coated substrate accessible to each receptor; and $(n_L - n_b)$ is the density of the unbound ligand. In the time interval Δt, two random numbers P_{rand1} and P_{rand2} between 0 and 1 are generated. The time interval Δt of 10 μs is used, as suggested by Ref. [5], to simulate leukocyte rolling for a period of 5 s. A new bond is formed under the condition $P_f > P_{rand1}$. On the other hand, an existing bond is ruptured when $P_r > P_{rand2}$. The simulation parameters used in this study are collected in Table I.

III. RESULTS

We first simulate a leukocyte rolling on a P-selectin-coated surface in a shear flow at a shear rate of $\gamma = 50\ \text{s}^{-1}$ (Reynolds number $\text{Re} = 5.86 \times 10^{-4}$), as shown in Fig. 1(b), and then compare the average translational velocity of the leukocyte with other existing simulation and experimental studies, as shown in Table II. Our results are calculated by a statistical ensemble average of five repeated independent runs. The same applies to other average physical quantities in this work. The simulation results for the rolling velocity agree with previously published data from other groups, indicating our approach is plausible.

Subsequently, in order to examine the effect of the flexural stiffness of microvilli, the simulations are conducted at the same conditions as the validation case, except that the flexural stiffness K is varied at three different levels: $0.1K_{\text{exp}}$, K_{exp}, and $10K_{\text{exp}}$ (see Table I) where $K_{\text{exp}} = 7\ pN/\mu\text{m}$ is the flexural stiffness of microvilli measured directly from the experiments [8]. The corresponding angle of microvilli, adhesive bonding force, number of receptor-ligand bonds, cell translational velocity, and cell deformation are computed and used to characterize the role of flexural stiffness K. It is important to note that in all the simulations the extensional stiffness is fixed at a constant value of 1340 pN/μm, so that our objective is to focus on the influence of flexural stiffness only.

In reference to the angle of microvilli, an angular distribution function $f(\theta)$ of the microvilli, those involved in adhesion, is defined and utilized to describe the probability of finding a microvillus

TABLE I. The simulation parameters used in this study.

Parameter	Definition	Value (experimental range)	Reference
ρ_f	Fluid density	1000 kg/m^3	[41]
μ_f	Fluid dynamic viscosity	0.0012 N s/m^2	[41]
D_{WBC}	Leukocyte diameter	7.5 μm	[42]
ρ_{WBC}	Leukocyte density	1077 kg/m^3	[5]
Y_{WBC}	Leukocyte membrane Young's modulus	300×10^{-6} N/m	[43]
K_{WBC}	Leukocyte membrane bending rigidity	3×10^{-18} J	[37]
k_f^0	Unstressed forward rate	1 s^{-1}	[44]
k_r^0	Unstressed reverse rate	1 s^{-1}	[44]
σ_b	Bond spring constant	1.0×10^{-3} N/m	[45]
σ_{ts}	Transition state spring constant	0.98×10^{-3} N/m	[45]
l_0	Equilibrium bond length	70 nm	[45,46]
K_B	Boltzmann constant	1.38×10^{-23} JK^{-1}	
T	Absolute temperature	310 K	[43]
	Number of PSGL-1 mol/cell	7500 molecules	[5]
	P-selectin site density	150 molecules/μm^2	[47,48]
N_{mv}	Number of microvilli	714	
L_{mv}	Microvillus length	0.35 μm	[49]
k_s^{mv}	Microvillus stiffness	1340 pN/μm (152–1340 pN/μm)	[50,51]
K_{exp}	Experimental microvillus flexural stiffness	7 pN/μm (4–7 pN/μm)	[8–10]

at an angle of θ per unit angle, and it is written as

$$f(\theta) = \frac{1}{\pi n} \sum_i \delta(\theta - \theta_i), \tag{7}$$

where n is the total number of the microvilli that adhere to the substrate and θ_i is the bending angle of the ith microvillus. The results of an ensemble average of the angular distribution function $\langle f(\theta) \rangle$ are displayed and compared in Fig. 2. The results indicate that when the flexural stiffness is the greatest, the angular distribution function has a high peak close to zero, suggesting that the most microvilli are oriented in the direction parallel to the angular baseline, which connects the mass center of the cell to the microvillus base and extends to the outside of the cell surface [see Fig. 1(a)]. As the flexural stiffness is reduced to a lower level, the peak becomes lower and wider, and shifts to a smaller angle around $\theta = 0.14\pi$, indicating that the microvilli are oriented away from the direction parallel to the angular baseline. As the flexural stiffness is continuously reduced to the lowest level, the peak is much lower and wider, around $\theta = 0.42\pi$, implying that the most microvilli are oriented to the direction perpendicular to the angular baseline and flatter with the substrate, as compared with the other two cases. Figures 3(a) and 3(b) show the snapshots of the cell in the simulations where the values of flexural stiffness of the microvilli are at $0.1K_{\text{exp}}$ and $10K_{\text{exp}}$, respectively. In the area close

TABLE II. Comparison of the average translational velocity of the leukocyte among different groups.

Source	Translational velocity $\pm$ std (μm/s)
Present results	2.017 ± 0.124
Pospieszalska *et al.* simulation [5]	3.42 ± 0.51
Pospieszalska *et al.* experiment [5]	1.52
Lawrence *et al.* experiment [52]	2.47–4.25

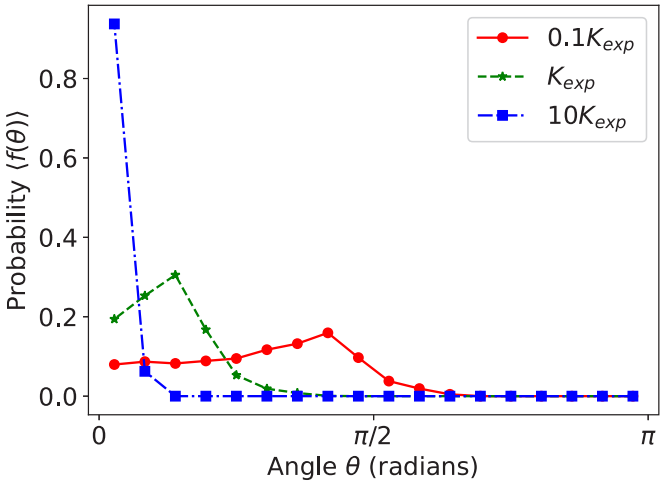

FIG. 2. The simulation results of the angular distribution of the microvilli at three different levels of the flexural stiffness.

to the substrate, as shown in Fig. 3(a), the leukocyte microvilli are lying on the substrate in a prone position, whereas, as shown in Fig. 3(b), the leukocyte microvilli stand more erectly on the substrate.

Next, receptor-ligand bonding forces are computed. Although a bonding force (direction and magnitude) is varied and depends on its location, the bonding force can be decomposed into two components in a local coordinate: one is parallel to the direction of the angular baseline [see Fig. 1(a)], and the other is perpendicular to it. The parallel force component of total bond force on the ith bonded microvillus $\mathbf{F}_{\parallel}^{\text{bond},i}$ is responsible for the extensional deformation of the microvillus, while the perpendicular force component of the total bond force on the ith bonded microvillus $\mathbf{F}_{\perp}^{\text{bond},i}$ is responsible for the bending deformation. Further, a total local coordinate-based bond force is defined by $F^{\text{bond}} = \langle \sum_i |\mathbf{F}^{\text{bond,i}}| \rangle$. Simultaneously, the corresponding total parallel component is

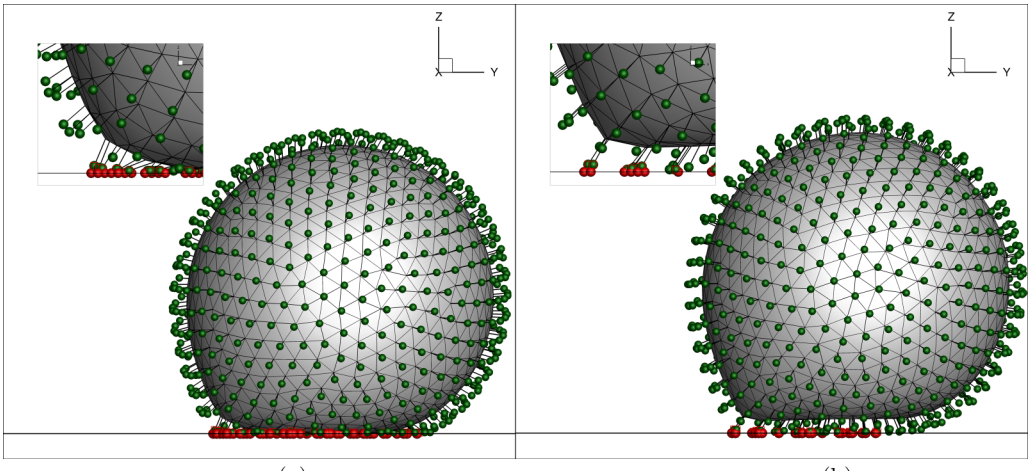

(a) (b)

FIG. 3. The snapshots of the simulations at two levels of the flexural stiffness of (a) $K = 0.1K_{\text{exp}}$ and (b) $K = 10K_{\text{exp}}$. The green and red points represent microvilli tips and the places where the receptor-ligand bonds are formed.

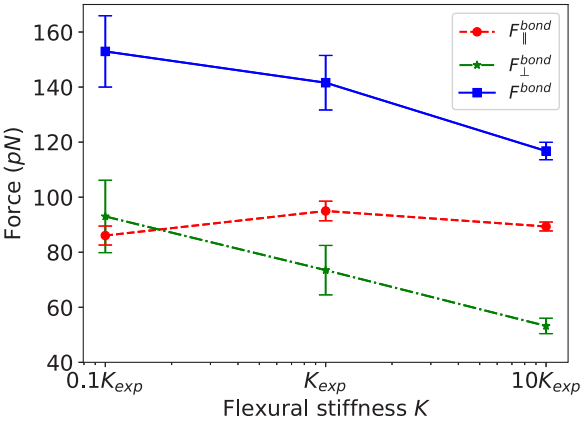

FIG. 4. The simulation results of the total local coordinate-based bond forces and their parallel and perpendicular components at three different levels of the flexural stiffness.

defined by $F_{\parallel}^{\text{bond}} = \langle \sum_i |\mathbf{F}_{\parallel}^{\text{bond},i}| \rangle$ and the total perpendicular component is defined by $F_{\perp}^{\text{bond}} = \langle \sum_i |\mathbf{F}_{\perp}^{\text{bond},i}| \rangle$. The two force components represent total extensional and bending actions on all the bonded microvilli. The results are plotted in Fig. 4, where $F_{\perp}^{\text{bond}}$ significantly increases as the flexural stiffness decreases. This is consistent with the fact that the bending angle significantly increases as the flexural stiffness decreases or the flexibility increases, since the flexibility is responsible for the bending deformation. However, $F_{\parallel}^{\text{bond}}$ remains approximately at the same level because the spring extensional stiffness is fixed at the same level. It is the flexibility of the microvillus which causes it to bend and leads to an increase in the perpendicular component. The increase in the total local coordinate-based bond force results mainly from the increase in the perpendicular component (see Fig. 4).

A receptor-ligand bond may be formed when a receptor and its ligand are very close to each other. If the microvilli are more flattened, due to bending, with the cell surface, the entire leukocyte will be closer to the substrate. Therefore, the PSGL-1 molecules on microvilli tips may bind more easily with the P-selectin molecules on the substrate. Conversely, if the microvilli on the cell bottom are erect, the microvilli tips are far away from the P-selectin on the substrate and may not form additional bonds. To quantify the number of the microvilli between the cell surface and substrate, λ_{mv} is defined as a ratio of the number of microvilli located within a critical height H_c to the total number of microvilli. The critical height is the distance above the substrate and is set to the unstressed equilibrium receptor-ligand bond length, $H_c = l_0 = 70$ nm. The ratio is used to evaluate the possible bonding. The larger the value of λ_{mv}, the more likely the number of microvilli are to attach and bind with the substrate, and vice versa. Figure 5(a) shows that the ratio λ_{mv} increases as the flexural stiffness decreases (or as the flexibility increases) because of alignment of the microvilli with the substrate.

To inspect the rolling behavior of the leukocyte, the ensemble average of the translational velocity was calculated, and the results are exhibited as a function of the flexural stiffness in Fig. 5(b). The result shows that as the flexural stiffness decreases, the translational rolling velocity of the leukocyte decreases due to the increase in the adhesive bonding force. Simultaneously, the ensemble average of the number of the receptor-ligand bonds was computed, and is displayed as a function of the flexural stiffness in Fig. 5(c). It shows that as the flexural stiffness decreases, the number of receptor-ligand bonds increases. It is clear that a decrease in the translational velocity is attributed to an increase in the number of receptor-ligand bonds and in the perpendicular component of the adhesive bonding force, due to the flexibility of the microvilli.

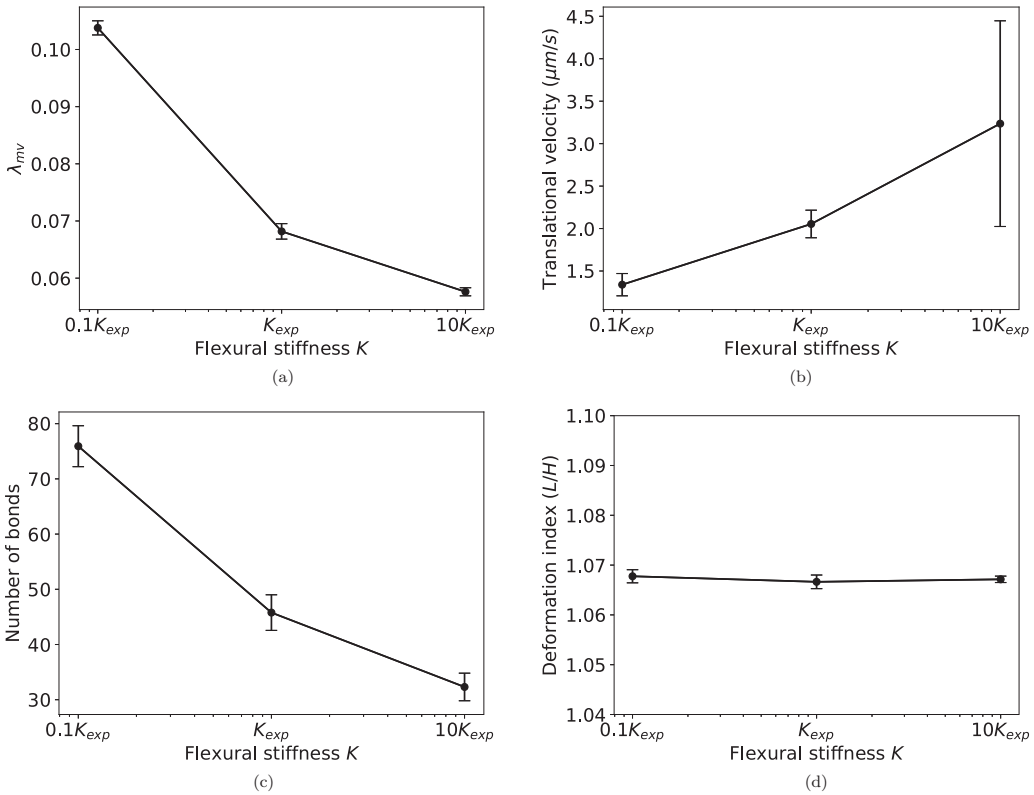

FIG. 5. The simulation results of four different physical properties at different levels of the flexural stiffness. (a) Ratio λ_{mv}, (b) Average translational velocity, (c) Number of bonds, and (d) Deformation index (L/H).

Finally, the cell deformation was probed. The deformation index is defined by the ratio of cell length L to cell height H, as portrayed in Fig. 1(b). The results of the deformation indexes, as a function of the flexural stiffness, are given in Fig. 5(d). The figure shows that the deformation indexes remain at the same level, suggesting that the cell deformation has no significant change and is not affected by the flexural stiffness. Therefore, the changes in the number of adhesion bonds and the perpendicular bonding force exerted on leukocytes are caused by the flexural stiffness, as evidenced in the previous section, and are not caused by the bulk cell deformation.

IV. CONCLUSION

This Rapid Communication studies the effects of the flexural stiffness of leukocyte microvilli on the rolling process related to the adhesion of leukocytes by using LLM and AD simulations. It is found that the flexural stiffness has a profound effect on rolling velocity and adhesive bonding force. It is demonstrated that the bending angles of the microvilli and the perpendicular component of the adhesive bonding force significantly increase as the flexural stiffness of the microvilli decreases, resulting in an increase in the number of receptor-ligand bonds and a decrease in the translational rolling velocity of leukocytes. It is the flexibility of the microvilli which results in their flattening on the substrate, expedites contact with the substrate, and facilitates the formation of adhesive bonds. Certainly, the influence of the flexural stiffness cannot be ignored. It is also shown that the flexural stiffness does not affect the bulk cell deformation.

ACKNOWLEDGMENTS

T.-H.W. would like to thank Western Michigan University for support via a Gwen Frostic Doctoral Fellowship, which helped him to finish this work. The authors also thank Marianne Di Pierro for manuscript advice.

[1] K. E. Caputo and D. A. Hammer, Effect of microvillus deformability on leukocyte adhesion explored using adhesive dynamics simulations, Biophys. J. **89**, 187 (2005).
[2] D. A. Hammer and S. M. Apte, Simulation of cell rolling and adhesion on surfaces in shear flow: General results and analysis of selectin-mediated neutrophil adhesion, Biophys. J. **63**, 35 (1992).
[3] P. Pawar, S. Jadhav, C. D. Eggleton, and K. Konstantopoulos, Roles of cell and microvillus deformation and receptor-ligand binding kinetics in cell rolling, Am. J. Physiol. **295**, H1439 (2008).
[4] D. B. Khismatullin and G. A. Truskey, A 3D numerical study of the effect of channel height on leukocyte deformation and adhesion in parallel-plate flow chambers, Microvasc. Res. **68**, 188 (2004).
[5] M. K. Pospieszalska, A. Zarbock, J. E. Pickard, and K. Ley, Event-tracking model of adhesion identifies load-bearing bonds in rolling leukocytes, Microcirculation **16**, 115 (2009).
[6] J.-Y. Shao, Biomechanics of leukocyte and endothelial cell surface, in *Leucocyte Adhesion*, Current Topics in Membranes Vol. 64 (Academic, New York, 2009), pp. 25–45.
[7] L. L. Munn, R. J. Melder, and R. K. Jain, Role of erythrocytes in leukocyte-endothelial interactions: mathematical model and experimental validation, Biophys. J. **71**, 466 (1996).
[8] D.-K. Yao and J.-Y. Shao, Flexibility of single microvilli on live neutrophils and lymphocytes, Phys. Rev. E **76**, 021907 (2007).
[9] D.-K. Yao and J.-Y. Shao, A novel technique of quantifying flexural stiffness of rod-like structures, Cell. Mol. Bioeng. **1**, 75 (2008).
[10] S. I. Simon, T. Nyunt, K. Florine-Casteel, K. Ritchie, H. P. Ting-Beall, E. Evans, and D. Needham, Dynamics of neutrophil membrane compliance and microstructure probed with a micropipet-based piconewton force transducer, Ann. Biomed. Eng. **35**, 595 (2007).
[11] P. Lallemand and L.-S. Luo, Theory of the lattice Boltzmann method: Dispersion, dissipation, isotropy, Galilean invariance, and stability, Phys. Rev. E **61**, 6546 (2000).
[12] S. Succi, *The Lattice Boltzmann Equation: For Fluid Dynamics and Beyond* (Oxford University Press, Oxford, 2001).
[13] Z. Guo and C. Shu, *Lattice Boltzmann Method and its Applications in Engineering* (World Scientific, Singapore 2013), Vol. 3.
[14] C. K. Aidun and J. R. Clausen, Lattice-Boltzmann method for complex flows, Annu. Rev. Fluid Mech. **42**, 439 (2010).
[15] D. Qi, Lattice Boltzmann simulations of particles in non-zero Reynolds number flows, J. Fluid Mech. **385**, 41 (1999).
[16] D. Qi, Direct simulations of flexible cylindrical fiber suspensions in finite Reynolds number flows, J. Chem. Phys. **125**, 114901 (2006).
[17] D. Qi, G. He, and Y. Liu, Lattice Boltzmann simulations of a pitch-up and pitch-down maneuver of a chord-wise flexible wing in a free stream flow, Phys. Fluids **26**, 021902 (2014).
[18] D. Qi and R. Gordnier, Effects of deformation on lift and power efficiency in a hovering motion of a chord-wise flexible wing, J. Fluids Struct. **54**, 142 (2015).
[19] D. L. Koch and A. J. Ladd, Moderate Reynolds number flows through periodic and random arrays of aligned cylinders, J. Fluid Mech. **349**, 31 (1997).
[20] C. Sun and L. L. Munn, Particulate nature of blood determines macroscopic rheology: A 2-D lattice Boltzmann analysis, Biophys. J. **88**, 1635 (2005).
[21] C. Sun and L. L. Munn, Influence of erythrocyte aggregation on leukocyte margination in postcapillary expansions: A lattice Boltzmann analysis, Physica A **362**, 191 (2006).

[22] M. M. Dupin, I. Halliday, C. M. Care, L. Alboul, and L. L. Munn, Modeling the flow of dense suspensions of deformable particles in three dimensions, Phys. Rev. E **75**, 066707 (2007).
[23] M. M. Dupin, I. Halliday, C. M. Care, and L. L. Munn, Lattice Boltzmann modelling of blood cell dynamics, Int. J. Comput. Fluid Dyn. **22**, 481 (2008).
[24] L. L. Munn and M. M. Dupin, Blood cell interactions and segregation in flow, Ann. Biomed. Eng. **36**, 534 (2008).
[25] D. A. Fedosov, B. Caswell, and G. E. Karniadakis, A multiscale red blood cell model with accurate mechanics, rheology, and dynamics, Biophys. J. **98**, 2215 (2010).
[26] T.-H. Wu, R.-S. Guo, G.-W. He, Y.-M. Liu, and D. Qi, Simulation of swimming of a flexible filament using the generalized lattice-spring lattice-Boltzmann method, J. Theor. Biol. **349**, 1 (2014).
[27] C. S. Peskin, The immersed boundary method, Acta Numerica **11**, 479 (2002).
[28] T.-H. Wu, M. Khani, L. Sawalha, J. Springstead, J. Kapenga, and D. Qi, A CUDA-based implementation of a fluid-solid interaction solver: The immersed boundary lattice-Boltzmann lattice-spring method, Commun. Comput. Phys. **23**, 980 (2018).
[29] D. D'Humieres, I. Ginzburg, M. Krafczyk, P. Lallemand, and L.-S. Luo, Multiple-relaxation-time lattice Boltzmann models in three dimensions, Philos. Trans. R. Soc., A **360**, 437 (2002).
[30] C. Pan, L.-S. Luo, and C. T. Miller, An evaluation of lattice boltzmann schemes for porous medium flow simulation, in *Proceedings of the First International Conference for Mesoscopic Methods in Engineering and Science* [Comput. Fluids **35**, 898 (2006)].
[31] Y. Tang, T.-H. Wu, G.-W. He, and D. Qi, Multi-flexible fiber flows: A direct-forcing immersed boundary lattice-Boltzmann lattice-spring approach, Int. J. Multiphase Flow **99**, 408 (2018).
[32] See Supplemental Material at http://link.aps.org/supplemental/10.1103/PhysRevFluids.3.031101 for a brief theory of the multi-relaxation-time lattice-Boltzmann method and a derivative of the relationship between the structure of the microvilli and the bending energy and elasticity.
[33] Y. Liu, T.-H. Wu, R.-S. Guo, Y.-H. Lee, and D. Qi, Dynamics of sedimentation of flexible fibers in moderate Reynolds number flows, Comput. Fluids **48**, 125 (2011).
[34] Y. Luo, T.-H. Wu, and D. Qi, Lattice-boltzmann lattice-spring simulations of flexibility and inertial effects on deformation and cruising reversal of self-propelled flexible swimming bodies, Comput. Fluids **155**, 89 (2017).
[35] D. A. Fedosov, J. Fornleitner, and G. Gompper, Margination of White Blood Cells in Microcapillary Flow, Phys. Rev. Lett. **108**, 028104 (2012).
[36] D. A. Fedosov and G. Gompper, White blood cell margination in microcirculation, Soft Matter **10**, 2961 (2014).
[37] D. A. Fedosov, *Multiscale Modeling of Blood Flow and Soft Matter* (Brown University, Providence, RI, 2010).
[38] E. Y. H. Park, M. J. Smith, E. S. Stropp, K. R. Snapp, J. A. DiVietro, W. F. Walker, D. W. Schmidtke, S. L. Diamond, and M. B. Lawrence, Comparison of PSGL-1 microbead and neutrophil rolling: Microvillus elongation stabilizes P-selectin bond clusters, Biophys. J. **82**, 1835 (2002).
[39] T.-H. Wu and D. Qi, Lattice-Boltzmann lattice-spring simulations of influence of deformable blockages on blood fluids in an elastic vessel, Comput. Fluids **155**, 103 (2017).
[40] M. Dembo, D. C. Torney, K. Saxman, and D. Hammer, The reaction-limited kinetics of membrane-to-surface adhesion and detachment, Proc. R. Soc. B **234**, 55 (1988).
[41] R. Skalak and S. Chien, *Handbook of Bioengineering* (McGraw-Hill, New York, 1987).
[42] P. Tandon and S. L. Diamond, Kinetics of β_2-integrin and l-selectin bonding during neutrophil aggregation in shear flow, Biophys. J. **75**, 3163 (1998).
[43] S. Jadhav, C. D. Eggleton, and K. Konstantopoulos, A 3-D computational model predicts that cell deformation affects selectin-mediated leukocyte rolling, Biophys. J. **88**, 96 (2005).
[44] P. Mehta, R. D. Cummings, and R. P. McEver, Affinity and kinetic analysis of p-selectin binding to P-selectin glycoprotein ligand-1, J. Biol. Chem. **273**, 32506 (1998).
[45] M. Dembo, On peeling an adherent cell from a surface, *Some Mathematical Problem in Biology*, in Lectures on Mathematics in the Lift Sciences, Vol. 24 (American Mathematical Society, Providence, RI, 1994), pp. 51–77.

[46] K. D. Patel, M. U. Nollert, and R. P. McEver, P-selectin must extend a sufficient length from the plasma membrane to mediate rolling of neutrophils, J. Cell Biol. **131**, 1893 (1995).

[47] K. L. Moore, K. D. Patel, R. E. Bruehl, F. Li, D. A. Johnson, H. S. Lichenstein, R. D. Cummings, D. F. Bainton, and R. P. McEver, P-selectin glycoprotein ligand-1 mediates rolling of human neutrophils on P-selectin, J. Cell Biol. **128**, 661 (1995).

[48] T. Yago, A. Leppänen, H. Qiu, W. D. Marcus, M. U. Nollert, C. Zhu, R. D. Cummings, and R. P. McEver, Distinct molecular and cellular contributions to stabilizing selectin-mediated rolling under flow, J. Cell Biol. **158**, 787 (2002).

[49] J.-Y. Shao, H. P. Ting-Beall, and R. M. Hochmuth, Static and dynamic lengths of neutrophil microvilli, Proc. Natl. Acad. Sci. USA **95**, 6797 (1998).

[50] D. B. Khismatullin and G. A. Truskey, Three-dimensional numerical simulation of receptor-mediated leukocyte adhesion to surfaces: Effects of cell deformability and viscoelasticity, Phys. Fluids **17**, 031505 (2005).

[51] Z. Y. Luo, S. Q. Wang, L. He, T. J. Lu, F. Xu, and B. F. Bai, Front tracking simulation of cell detachment dynamic mechanism in microfluidics, Chem. Eng. Sci. **97**, 394 (2013).

[52] M. B. Lawrence and T. A. Springer, Leukocytes roll on a selectin at physiologic flow rates: Distinction from and prerequisite for adhesion through integrins, Cell **65**, 859 (1991).